small
NANO MICRO

Biomolecule-Doped PEDOT with Three-Dimensional Nanostructures as Efficient Catalyst for Oxygen Reduction Reaction

Zhaoyan Guo, Huan Liu, Congcong Jiang, Ying Zhu,* Meixiang Wan, Liming Dai, and Lei Jiang*

***M**etal macro-cyclic compounds have drawn considerable attention as alternative catalysts for oxygen reduction reaction. However, the continuous pyrolysis process usually needed for improving the performance of these compounds require an elevated temperature and complicated procedures, thus leading to an unpredictable transformation of the chemical structures and limiting their applications. Herein, we develop a new insight to fabricating hemin-doped poly (3,4-ethylenedioxythiophene) (PEDOT) with controllable three-dimensional nanostructures via a one-step, tri-phase, self-assembled polymerization routine. We demonstrate that the hemin-induced synergistic effect results in a very high 4-electron oxygen reduction activity, a better stability, and free from methanol crossover effects even in a neutral phosphate buffer solution (PBS).*

1. Introduction

As an essential cathode reaction in fuel cells and metal-air batteries, the oxygen reduction reaction (ORR) with its sluggish kinetics has been considered to be a major limiting factor to the associated energy-conversion efficiency.[1,2] Although platinum (Pt)-based catalysts have been so far the most active ORR catalysts, their high cost and scarcity, poor long-term stability, and susceptibility to the MeOH crossover/CO-poisoning effects have severely hindered large-scale commercialization of fuel-cell technology.[2] To reduce the use of expensive Pt in fuel cells, considerable efforts have been devoted to rational design and fabrication of non-precious metal catalysts with unique architectures for high ORR activities. In the early 1960's, Jasinski demonstrated that cobalt phthalocyanine could act as electro-catalyst for oxygen reduction. This inspiring finding has triggered extensive research to develop various transition-metal macro-cyclic compounds as potential alternative catalysts for ORR.[3–5] As many bio-molecules contain transition-metal macro-cyclic units in their skeleton for certain biological functions,[6–12] the use of bio-molecules with innate reactive sites for ORR has recently been proven to be an effective approach to high-performance non-precious-metal ORR catalysts.[8–16] For example, vitamin B12 with a naturally active Co-N_x-C center was adsorbed on carbon black and followed by pyrolysis to show favorable ORR performance with a high durability.[8] Recent efforts have also demonstrated that adsorbed hemin, a bio-molecule with Fe-N_4-C structure, on carbon black or graphene nano-plates as the conducting support enabled effective ORR catalysts.[9,10,15,17] However, some key issues

Z. Guo, Dr. H. Liu, C. Jiang, Prof. Y. Zhu
Key Laboratory of Bio-inspired Smart Interfacial Science and Technology of Ministry of Education
School of Chemistry and Environment
Beihang University
Beijing 100191, P.R. China
Fax: +86 10–82338212
E-mail: liuh@buaa.edu.cn; zhuying@buaa.edu.cn
Prof. M. Wan, Prof. L. Jiang
Beijing National Laboratory for Molecular Sciences
Institute of Chemistry Chinese Academy of Sciences
Beijing 100190, P.R. China
Prof. L. Dai
Department of Macromolecular Science and Engineering
Case Western Reserve University
10900 Euclid Avenue, Cleveland, Ohio 44106, United States

DOI: 10.1002/smll.201303642

remain unsolved so far. First, the chemical structures of the active centers in these macro-cyclic catalysts undergo complicated and unpredictable transformations during the pyrolysis process, making the rational design of them very difficult, if not impossible.[17] Second, the performance of these macro-cyclic ORR catalysts is competitive with that of Pt-based catalysts in alkaline or acid medium, but not in neutral electrolytes required for microbial fuel fells.[10,15] It remains a big challenge to develop a facile route to fabricate non-precious-metal ORR catalysts with comparable catalytic performances to Pt-based catalysts under neutral conditions.

On the other hand, heterocyclic conjugated polymers, including polyaniline, polypyrrole, and poly(3,4-ethylenedioxythiophene) (PEDOT), have recently been investigated as inexpensive non-precious-metal ORR electro-catalysts because of their low cost, high electronic conductivity, and distinct redox properties.[18–21] Generally speaking, these polymers can act as ORR electro-catalysts in the following three ways: 1) as catalysts on their own,[21] 2) as precursors for pyrolyzed M-N_x/C catalysts,[22] and 3) as matrix for entrapping non-precious metals.[18] Among them, the report by Winther-Jensen is of particular interest, in which the authors demonstrated that vapor-phase-polymerized PEDOT on a porous Goretex membrane exhibited high ORR performance with a better durability than the precious Pt catalyst.[21] Our previous research also suggested that hierarchically micro/nano-structured PEDOT could act as an efficient ORR catalyst over a wide pH range.[23] The high porosity and micro/nano-structures provide large surface areas for electrochemical reactions whereas the conductive PEDOT offers a low ohmic drop across the electrode.

In this study, we developed a one-step, H_2O/dimethylformamide (DMF)/3,4-ethylenedioxythiophene (EDOT) tri-phase self-assembling method to produce hemin-doped PEDOT with controllable three-dimensional hierarchical structures, in which the ORR-active PEDOT served also as a conductive medium, after the hemin-doping, to support the non-precious-metal macro-cyclic ORR reactive centers (i.e., Fe-N_4-C) in hemin. The exploitation of the hemin-doped PEDOT composites as an effective ORR catalyst is based on the following rationales: 1) Hemin has been proven to be the actual oxygen hunter and combiner in the oxygen-transport-process of all vertebrates bodies, with oxygen molecules being combined directly to the iron centre of Fe-N_4-C active sites for ORR.[7,24] 2) The carboxyl groups within the hemin molecules are employed as doping ions to link with the PEDOT main chains by electrostatic interaction, rather than being weakly absorbed through physical sorption. 3) PEDOT shows a good electronic conductivity after doping, and thus can serve as an excellent charge collector and electron shuttle.[25] 4) PEDOT with its micro/nanostructures over a large surface area can itself be an outstanding intrinsic ORR catalyst over a wide pH range, including pH 7.[23] Our results demonstrate that the hemin-induced synergistic effects result in a very high ORR activity and stability. The hemin-doped PEDOT catalyzed a 4-electron ORR process with an activity that was beyond that of both pure PEDOT and hemin with a more positive onset potential and free from the methanol crossover effect even in a neutral phosphate buffer solution (PBS).

2. Results and Discussion

Figure 1 schematically shows the procedures for the preparation of the hemin-doped PEDOT hierarchical structures by self-assembly using a H_2O/DMF/EDOT tri-phase system. As is well known, DMF is an excellent aprotic polar solvent that is miscible with water in all volume proportions. EDOT is hardly soluble in water, but dissolves well in DMF, whereas ferric chloride as oxidant dissolves in water to become oxidative Fe^{3+}. Upon the addition of the EDOT/DMF mixture into the aqueous solution of $FeCl_3$ oxidant, therefore, a stable emulsion of H_2O/DMF/EDOT mixtures formed with EDOT droplets dispersed in polar water solution (inset of Figure 1). When the emulsion mixture was heated in the presence of $FeCl_3$ at 70 °C for 5 hours, oxidants (i.e., Fe^{3+}) in the aqueous phase induced the nucleation and polymerization of EDOT at the interface of the EDOT droplets. Because PEDOT is a rigid macromolecule, the EDOT droplets tended to fuse along the direction of the newly formed polymer chain during the polymerization process. Thus, the polymer chains can act as templates for the formation of brush-like nanorods (Figure 1) during the self-assembly/polymerization process. Hydrogen bonding between DMF and water may serve as the driving force behind the aggregation of EDOT droplets for the formation of junctions through the self-assembly process, as hydrogen bonding interactions have been previously demonstrated to play a key role in the formation of conducting polymer dendrites.[26] When the hemin molecules were introduced, the two hydrophilic carboxyl groups of the hemin molecule can not only act as dopants to the PEDOT chain, but also provide hydrogen bonding and π–π interactions to further aggregate EDOT droplets to form polymeric dendrites. If hemin is in excess in the polymerization process, however, the hemin residues could break the emulsion's stability, leading to the formation of irregular structures.

Figure 2 shows typical environmental scanning electron microscopic (ESEM) images for the as-prepared pristine PEDOT (a, b), PEDOT-hemin1 (c, d), PEDOT-hemin10 (e, f), and PEDOT-hemin20 (g, h). (Here, the X in PEDOT-heminX indicates X mM hemin was used for 1.87 mmol EDOT in 20 mL solution during the polymerization process. Details can be found in Supporting Information). As shown in Figure 2a, PEDOT without hemin consists of two-headed brush-like structures with the length of 500 nm and the top diameter of 150 nm. The magnified image (Figure 2b) exhibits that brush-like structures are composed of several nano-rods, which are bound tightly in the middle. As can be seen in Figure 2c-h, the addition of hemin in the reaction system leads to distinct changes in morphology of the as-prepared PEDOT nanostructures. For PEDOT-hemin1, Figure 2c shows relatively wide two-headed broom-like structures with an average length of the consisting brooms of about 850 nm and the diameter of the branched ends of about 350 nm. The magnified ESEM image in Figure 2d further reveals the middle of the broom-like structures is tight enough with both of the ends spreading out. Each of the ends consists of hundreds of nano-rods with a diameter of about 25 nm (Figure 2d). For PEDOT-hemin10, however, Figure 2e shows a flower-like structures composed of hierarchical

DOI: 10.1002/smll.201303642

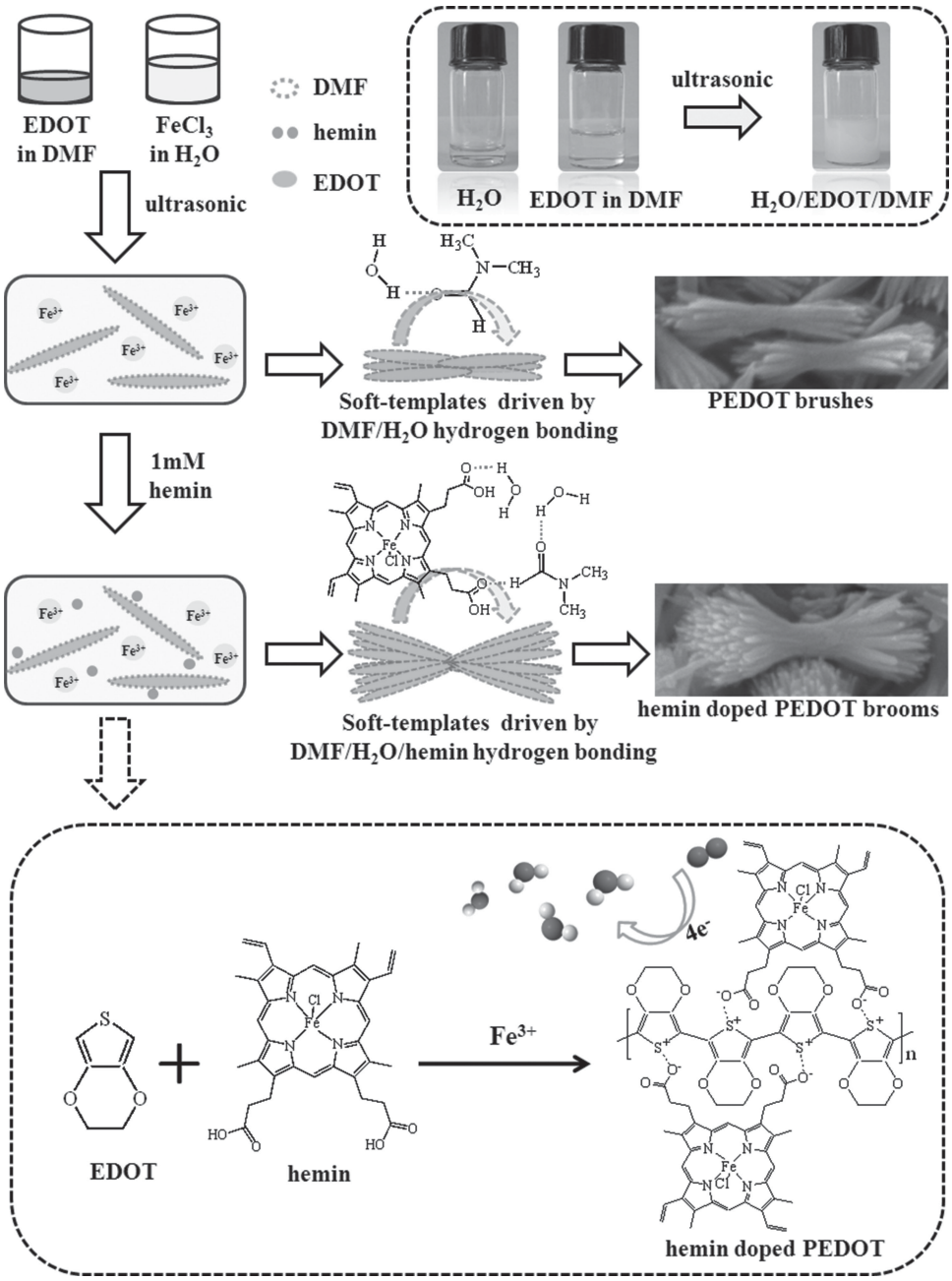

Figure 1. The self-assembling route to PEDOT and PEDOT-hemin nanostructures.

bunches with a diameter of about 100 nm radiated out from a common center (Figure 2f). For PEDOT-hemin20 and PEDOT-hemin25 with further increased amounts of hemin, inhomogeneous morphologies with brook-like and spherical structures are observed (Figure 2g and h, Figure S1). To understand effect of the hierarchical structures on the ORR activity, the specifically surface areas, including PEDOT and PEDOT-hemin, were measured by BET method using nitrogen adsorption-desorption isotherms. As shown in Table S1, all the samples have BET surface areas of 53–40 $m^2 \cdot g^{-1}$, which will be beneficial for ion adsorption and catalytic reactions. These results indicate that the hierarchical structures and surface areas of the as-prepared hemin-doped PEDOT can be tuned to tailor properties for specific applications (e.g., ORR) by adjusting the amount of hemin used in the polymerization process.

The chemical compositions of the as-prepared PEDOT and hemin-doped PEDOT (PEDOT-hemin) samples were investigated by X-ray photoelectron spectroscopic (XPS) measurements (**Figure 3**). As expected, the XPS spectra of PEDOT and PEDOT-hemins contain peaks for C, S and O, along with weak bands for Fe and Cl (Figure 3a). The appearance of the XPS Cl peak is mainly due to the presence of Cl^{-1}, from hydrolysis of $FeCl_3$, as doping ions into the PEDOT main chains. The nitrogen contents measured by XPS increased with increasing hemin concentrations to be 0.56, 1.77, 2.68 and 4.16 at% for PEDOT-hemin1, PEDOT-hemin10, PEDOT-hemin20 and PEDOT-hemin25,

DOI: 10.1002/smll.201303642

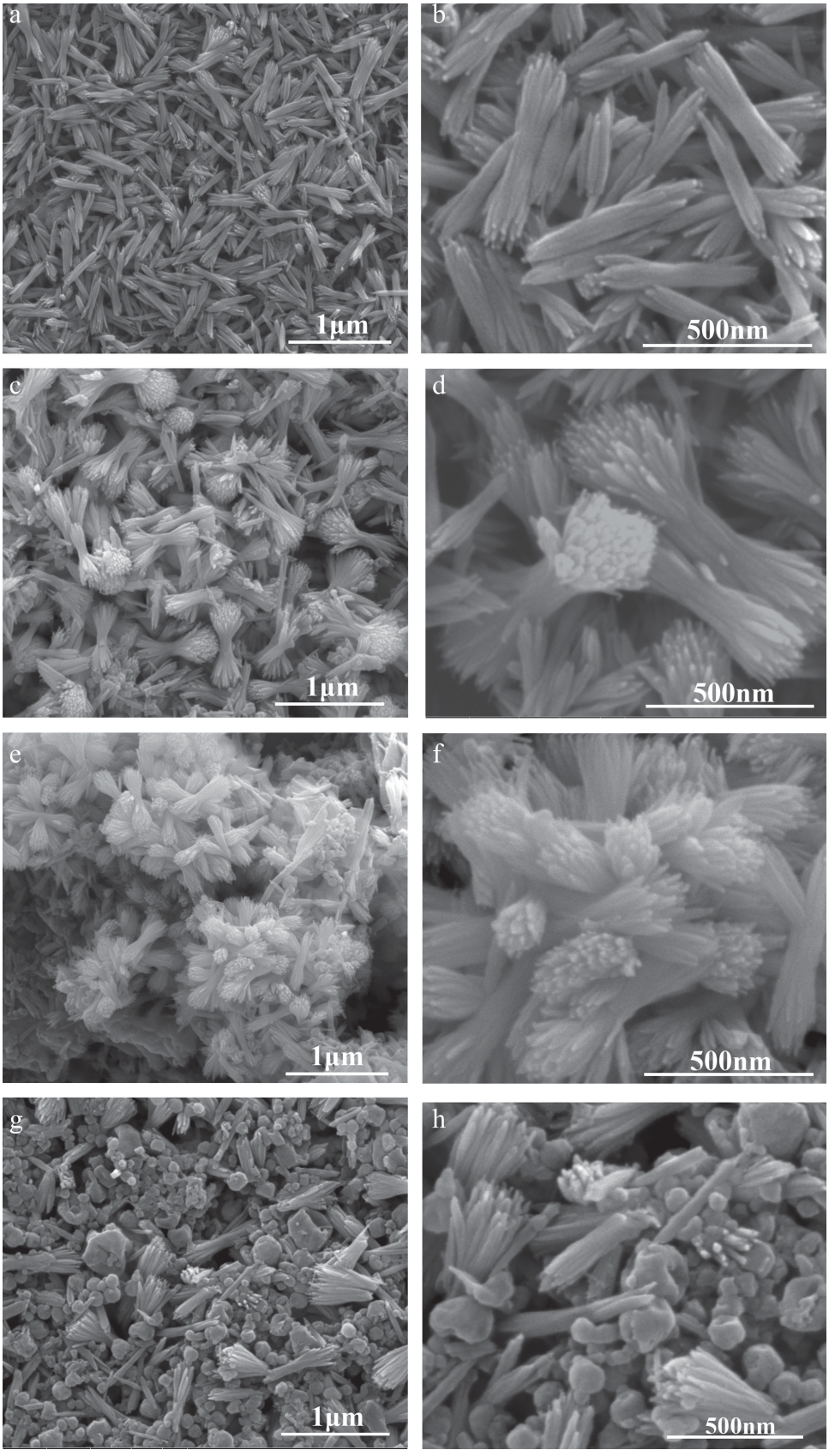

Figure 2. Typical ESEM images of PEDOT (a, b), PEDOT-hemin1 (c, d), PEDOT-hemin10 (e, f), and PEDOT-hemin20 (g, h).

small 2014,
DOI: 10.1002/smll.201303642

small NANO MICRO

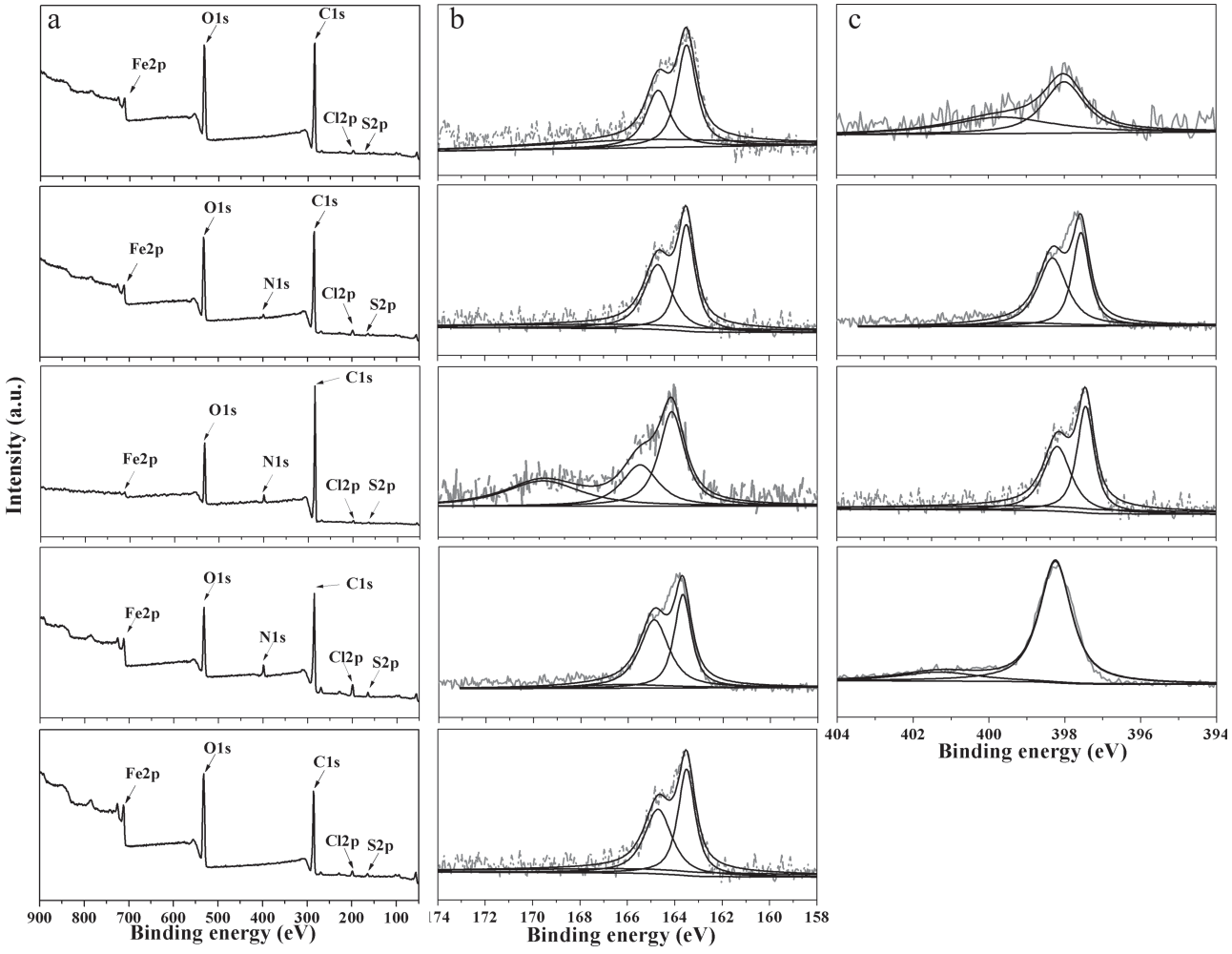

Figure 3. The XPS survey(a), S2p (b), N1s (c) core-level spectra with curve-fitting of PEDOT-hemin1, PEDOT-hemin10, PEDOT-hemin20, PEDOT-hemin25 and PEDOT(none nitrogen) (from top to bottom).

respectively (Figure 3c and Table S2). However, the N:S atomic ratio measured by XPS for PEDOT and PEDOT-hemins showed a maximum value (1.72) at the hemin concentration of 20 mM, indicating that the doping level of hemin increased with increasing hemin concentration and then leveled off at 20 mM. The observed highest atomic ratio of N:S (1.72:1) is still lower than the maximum theoretical value (2:1, Figure 1) because of the coexistence of Cl^--doping (Figure 3a and Table S2).

Further evidence for the chemical doping of hemin into PEDOT comes from FT-IR measurements. As shown in Figure S2, the FT-IR spectrum of EDOT (curve 0) is in accordance with previous reports.[27] The FT-IR spectrum of PEDOT (curve 1) shows characteristic peaks at 1540 and 1519 cm^{-1} due to $\nu_{C\alpha = C\beta}$ asymmetric stretching, as well as peaks at 1337 cm^{-1} attributable to the C_β-C_β stretching. Besides, the peaks at 1203 and 1092 cm^{-1} can be assigned to the C-O-C stretching in the ethylene dioxy groups while vibration bands at 981 and 844 cm^{-1} are due to the C-S stretching ($\nu_{C\text{-}S}$) in thiophene groups.[27–29] As can be seen from curve 6 in Figure S2., hemin shows a sharp band at 1700 cm^{-1} due to the C = O stretching of carboxyl groups, along with a small peak at 1630 cm^{-1} attributable to the $\nu_{10}(C_\alpha–C_\beta)$ band of the porphyrin skeleton.[30] The corresponding spectra of the as-prepared PEDOT-hemin1, 10, 20, and 25 (curve 2, 3, 4 and 5) also display the characteristic peaks of PEDOT. However, the peaks at 1640 cm^{-1} become stronger and shift to higher wavenumbers from PEDOT-hemin1 to 20 caused by doping of hemin molecules, along with Cl^-, into the PEDOT backbones. The adsorption peak at 1640 cm^{-1} in the FT-IR spectrum of PEDOT has been attributed to the doping effect and usually enhanced with increasing doping level.[31] Along with the peak at 1640 cm^{-1} becoming stronger and shifting to greater wavenumber from PEDOT-hemin1 to 20, a new peak around 1700 cm^{-1} appears. However, the spectrum of PEDOT-hemin25 (curve 5 of FigureS2) is almost identical to that of PEDOT-hemin20. These results indicate that more hemin molecules are associated with the PEDOT backbones as doping anions at a higher doping level at 20 mM, in consistent with the XPS results.

Electro-catalytic properties of the PEDOT and PEDOT-hemins were tested by cyclic voltagrammetry (CV) in aqueous

DOI: 10.1002/smll.201303642

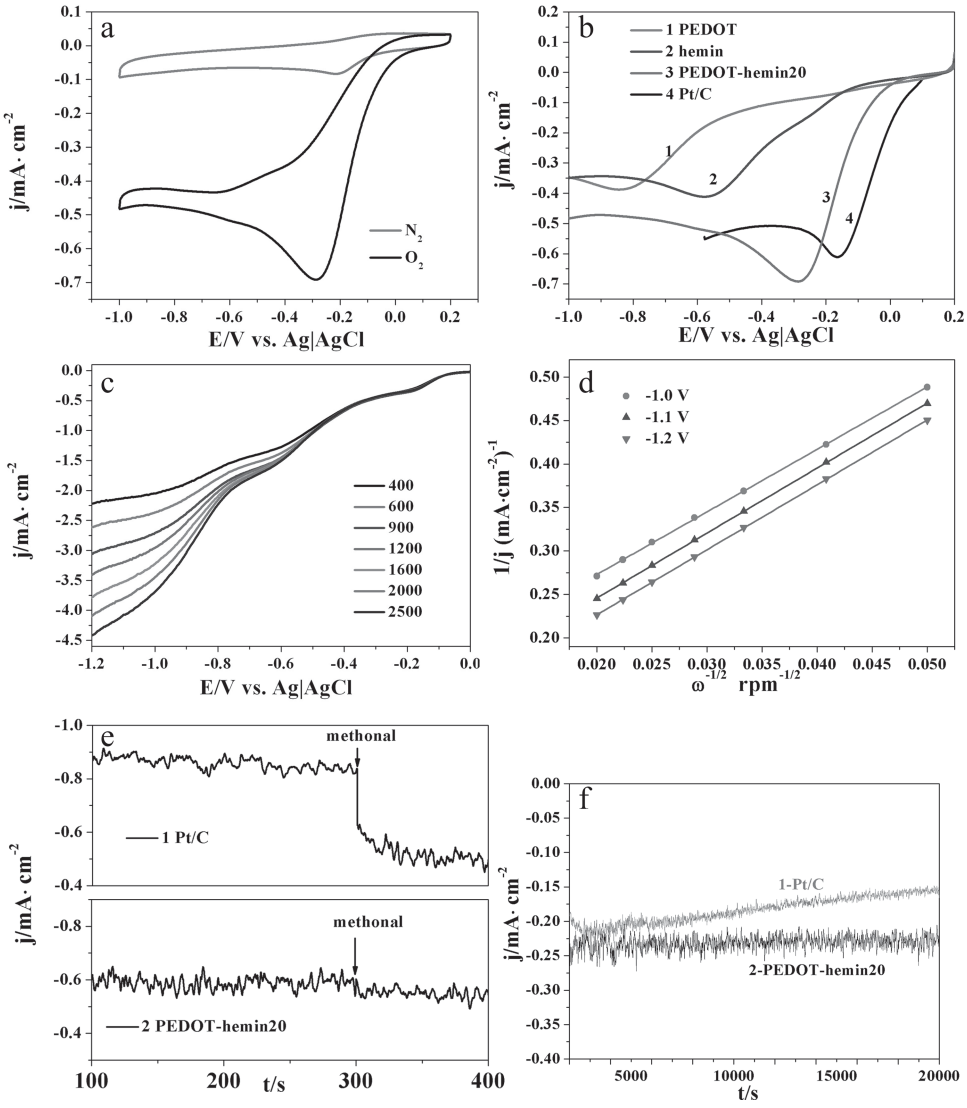

Figure 4. (a) The CV curves of the as-casted PEDOT-hemin20 on a GC electrode in 0.1 M PBS solution saturated with N_2 or O_2 at a scan rate of 50 mV.s^{-1}. (b) The CV curves of PEDOT, hemin, and PEDOT-hemin20 in O_2 saturated PBS solutions at a scan rate of 50 mV.s^{-1}. (c, d) The LSVs and the K-L plots of PEDOT-hemin20 at different rotation speeds. (e) The cathodic ORR catalytic current on the Pt/C electrode (line 1) and PEDOT-hemin20 (line 2) upon methanol injection. (f) The time course of Pt/C(line1) and PEDOT-hemin20(line2) electrode at constant potential under O_2 aeration condition for 5 hours.

phosphate buffer solutions (PBS) saturated with either N_2 or O_2, as shown in **Figure 4**a and b. Figure 4a presents CV curves of the as-casted PEDOT-hemin20 on a glass carbon (GC) electrode in 0.1 M PBS solution saturated with N_2 or O_2 at a scan rate of 50 mV·s^{-1}. As can be seen, an apparent reduction peak at the potential of –0.29 V (vs. Ag|AgCl) was observed for the PEDOT-hemin20 electrode in the O_2-saturated electrolyte solution, but not for the N_2-saturated solution, indicating that PEDOT-hemin20 can effectively catalyze cathodic oxygen reduction reaction. Figure 4b compares the CV curves for PEDOT, hemin, PEDOT-hemin20 and commercial Pt/C in the oxygen saturated electrolytes, which clearly shows that the ORR catalytic performance increase remarkably by doping PEDOT with hemin due to the synergistic ORR catalytic effect between hemin and PEDOT (vide supra). Generally speaking, positive shifting of the reduction potential indicates the decreasing of overpotential to initialize the ORR at the cathode.[32] Thus, the peak potential shift from the pure PEDOT (–0.85 V) through hemin (–0.56 V) to PEDOT-hemin20 (–0.29 V) indicates that oxygen reduction reaction on the PEDOT-hemin20 electrode can be effectively driven by a lower external energy. Moreover, PEDOT-hemin20 electrode exhibits a much higher ORR current density (0.69 mA·cm^{-2}) than that of the pure PEDOT (0.39 mA·cm^{-2}) and hemin (0.41 mA· cm^{-2}), which is slightly less than that of Pt/C catalyst (curve 4). Clearly, therefore, the PEDOT-hemin20 electrode possesses a much higher electro-catalytic activity than both PEDOT and hemin due, once again, to synergistic effect of doping PEDOT with hemin mentioned above. As shown in Figure S3, the cathodic reduction peaks show a positive shift with concomitant increase in the peak current densities roughly in the order from PEDOT, hemin, PEDOT-hemin1, PEDOT-hemin10 and PEDOT-hemin25, indicating that doping biological hemin

DOI: 10.1002/smll.201303642

molecules into PEDOT backbones causes an increase in the catalytic performance of pure PEDOT with increasing hemin doping level, and that hemin-doped PEDOT shows a superior ORR performance to both pure PEDOT and hemin due to the doping-induced synergistic effect.[30] Therefore, the bio-doped PEDOT shows promise as potential substitutes for noble-metal catalysts.

To further investigate the ORR performance, we carried out the linear sweep voltammetry (LSV) measurements for PEDOT-hemins, PEDOT and hemin, respectively, on a rotating disk electrode (RDE) in an O_2 saturated 0.1 M PBS electrolyte solution. Figure 4c shows the LSV curves at various rotation rates for PEDOT-hemin20. PEDOT-hemin20/GC electrode shows a three-step process with the onset potential of about –0.07 V, –0.23 V and –0.70 V. We atrribute the first slow step at –0.07 V to the reduction of high-valence iron (Fe^{IV}-$^2O_2^{2-}$, 12% in oxyheme) in hemin,[7] while the following two steps shoud be attributed to the two process of oxygen reduction. The limiting current density increased with increasing rotation rate, indicating the occurrence of a diffusion-controlled reaction on the electrode surface. The transferred electron number per oxygen molecule was determined by Koutechy-Levich equation as given below (Equation (1) and (2):

$$\frac{1}{j} = \frac{1}{j_k} + \frac{1}{B\omega^{0.5}} \quad (1)$$

$$B = 0.2nF(D_{O_2})^{2/3}\nu^{-1/6}C_{O_2} \quad (2)$$

where, j_k is kinetic current and ω is rotating rate. B can be determined by the slope of K-L plots based on Levich equation where n, F, D_{O2}, ν, C_{O2} represent the transferred electron number per oxygen molecule, Faraday constant (96485 C·mol^{-1}), diffusion coefficient of O_2 (1.9×10^{-5} cm^2·s^{-1}), the kinetic viscosity (1.1×10^{-2} cm^2·s^{-1}), and the bulk concentration of O_2 (1.2×10^{-6} mol·cm^{-3}) in PBS, respectively. The constant 0.2 is adopted when the rotation speed is expressed in rpm.[33] As shown in Figure 4c and d, the linear relationship between j^{-1} and $\omega^{-0.5}$ at different potentials can be clearly seen. The transferred number of electrons per O_2 molecule (n) calculated from the slope of K-L plots in Figure 4d is 3.8, indicating an almost 4-electron pathway for the ORR process catalyzed by PEDOT-hemin20. As a comparison, the transferred electron number of ORR catalyzed by PEDOT is calculated to be 2.3 (Figure S4a and b), suggesting a low-efficient ORR process with mixed two-electron and four-electron pathways to produce massive hydrogen peroxides as harmful by-product. The calculated transferred electron numbers for PEDOT-hemin1, PEDOT-hemin10 and PEDOT-hemin25 are 2.9, 3.6 and 3.7, respectively (Figure S4), which, once again, shows that the ORR catalytic activity of PEDOT-hemins increases with increasing hemin-doping level. The observed effcient catalytic properties of PEDOT-hemins are resulted from the following combined effects. As a well-known oxygen-binder and oxygen-transport reagent in biological systems, hemin molecules can effectively capture and bind oxygen molecules from aqueous solutions with oxygen binding on Fe^{3+} of the porphyrin skeleton.[7,24] Due to its poor conductivity, however, there is insufficient electron transfer from the charged GC electrode to the active centers of hemin to reduce the captured oxygen molecules, thus an inefficient 2-electron pathway for ORR catalyzed by hemin (Figure S4i and j). The chemical-doping hemin molecules into PEDOT significantly facilitates the electron transfer from the doped PEDOT to the active Fe-N_4-C centers of hemin to effectively reduce the H_2O_2 intermediate, if any produced by both PEDOT backbones and hemin, into H_2O before diffusion into the solution, and hence a 4-electron pathway for ORR catalyzed by PEDOT-hemins.

The PEDOT-hemin20 electrode was further subjected to testing the possible methanol crossover effect and stability towards ORR by measuring the chronoamperometric current-time (i-t) for ORR at the PEDOT-hemin20 electrode under appropriate conditions. As shown in Figure 4e, the cathodic ORR catalytic current on the PEDOT-hemin20 electrode keeps constant upon the injection of methanol (indicated by the arrow, Figure 4e, line 2), whereas that on the Pt/C electrode decreased sharply by about 44% (indicated by the arrow, Figure 4e, line 1). Clearly, therefore, the PEDOT-hemin20 has higher fuel selectivity towards ORR than the commercial Pt/C electro catalysts. The durability of the PEDOT-hemin20 for ORR was also evaluated via a chronoamperometic method at –0.3 V in an air-saturated 0.1 M PBS. As seen in Figure 4f, the cathodic current of PEDOT-hemin20 electrode current can keep constant with continuous operation for 5 hours while that of Pt/C electrode decreased by 33%.

3. Conclusion

In conclusion, we have developed a new class of efficient non-precious-metal ORR catalysts by doping PEDOT with hemin via a one-step, H_2O/DMF/EDOT tri-phase self-assembling. It is demonstrated that the hemin-induced synergistic effect results a very high 4-electron ORR activity, a better stability, and free-from methanol crossover effect even in a neutral phosphate buffer solution (PBS) due to hemin molecular characteristic, in which the iron centre of Fe-N_4-C served for ORR,while the carboxyl groups used dopant for conducting PEDOT. We therefore envision that this bio-molecule doped PEDOT will open a new avenue for the design and development of novel non-precious-metal ORR catalysts with higher efficiency and good stability, particularly in neutral electrolytes.

4. Experimental Section

Materials: 3,4-ethylenedioxythiophene (EDOT) monomer was purchased from Sigma-Aldrich and used without further purification. Hemin was purchased from Frontier Scientific, Inc. Other reagents, including $FeCl_3$, NaH_2PO_4, Na_2HPO_4, dimethylformamide (DMF) and ethanol, were of analytical grade and used without further purification. Nafion (DuPont, 10 wt%) was diluted to 0.05 wt% by ethanol. Pt/C (20 wt%) catalyst was purchased from the Johnson Matthey Company.

DOI: 10.1002/smll.201303642

Chemical polymerization of PEDOT: PEDOT was synthesized in 20 mL mixed solvents of DMF and water with an optimized volume ratio of 1:3 with $FeCl_3$ as the oxidant. In a typical synthetic procedure, $FeCl_3$ was dissolved into 15 mL de-ionized water while 0.2 mL (1.87 mmol) EDOT monomer and a predetermined amount of hemin was dissolved into 5 mL DMF. After dispersing these two solutions by ultrasonic separately for 2 minutes, they were mixed together. After dispersion by ultrasonic for 30 seconds, the mixture was put into a water bath (HH-6, Beijing) under 70 ºC for 5 hours. The resulting precipitate was sequentially washed with water, DMF and methanol for several times and separated by centrifuging, and finally dried in a dynamic vacuum at room temperature for 48 hours.

Morphology and Molecular Characterization: The morphology of the PEDOT powder was measured by environmental scanning electron microscopy (ESEM, Quanta 250 FEG). The samples for the ESEM imaging were prepared by placing a drop of the sample suspended in ethanol on a silicon slide.

Molecular structures of the polymerized products were characterized by Fourier transform infrared spectra (FT-IR), and X-ray photoelectron spectroscopy (XPS). FT-IR spectra were recorded on a Varian 3100 FT-IR spectrophotometer (Excalibur Series) using KBr pressed disks. XPS spectra from the as-synthesized PEDOT and PEDOT-hemins were measured on a VG ESCALAB 220i-XL instrument with a monochromatic AlKα X-ray source. Nitrogen sorption/desorption measurements were performed with ASAP 2020M (Micromeritics, USA) to obtain BET-specific surface area.

Electrochemical characterization: Cyclic voltammetry (CV) measurements were conducted on a computer-controlled electrochemical workstation (CHI 760D, Shanghai) with a standard three-electrode electrochemical cell equipped with a gas flow system. A glass carbon (GC) electrode coated with PEDOT, hemin, or PEDOT-hemins was used as the working electrode, an Ag|AgCl (KCl sat.) electrode as the reference electrode, and a platinum wire as the counter electrode. The rotating disk electrode (RDE) voltagrammetry experiments were performed by linear sweep voltagrammetry (LSV) on an electrode rotator (AFMSRCE, Pine) and recorded by an electrochemical analyzer (CHI 660D, Chenhua, Shanghai). For all CV and RDE measurements, an aqueous solution of 0.1 M phosphate buffer solution (PBS, pH = 7) was used as the electrolyte. N_2 or O_2 was used to purge the solution to achieve oxygen-free and oxygen-saturated electrolyte solutions.

The working electrode for CV was prepared as follows: prior to use, the working electrode was polished with alumina slurry to obtain a mirror-like surface and then washed with deionized water before drying up. A portion of 2 mg of catalyst was dispersed in 1 mL of ethanol by sonication for 10 min. Then, 15 µL of the dispersion was transferred onto the GC electrode by using a microsyringe, followed by dropping 5 µL of Nafion solution in ethanol (0.05 wt.%).

Supporting Information

Supporting Information is available from the Wiley Online Library or from the author.

Acknowledgements

The work is supported by the National Natural Science Foundation of China (51273008), the the National Basic Research Program (2012CB933200), the National High-Tech Research and Development Program (2012AA030305), and the Fundamental Research Funds for the Central Universities (YWF-10–01-B16).

[1] M. S. Whittingham, T. Zawodzinski, *Chem. Rev.* **2004**, *104*, 4243.
[2] M. Winter, R. J. Brodd, *Chem. Rev.* **2004**, *104*, 4245.
[3] B. Das, M. Mandal, A. Upadhyay, P. Chattopadhyay, N. Karak, *Biomed. Mater. (Bristol, England)* **2013**, *8*, 035003.
[4] G. Ghodake, S. R. Lim, D. S. Lee, *Colloid. Surface. B* **2013**, *108*, 147.
[5] F. Touti, P. Maurin, J. Hasserodt, *Angew. Chem. Int. Ed.* **2013**, *52*, 4654.
[6] J. J. Katz, J. R. Norris, L. L. Shipman, M. C. Thurnauer, M. R. Wasielewski, *Annu. Rev. Biophys. Bioeng.* **1978**, *7*, 393.
[7] K. P. Jensen, B. O. Roos, U. Ryde, *J. Inorg. Biochem.* **2005**, *99*, 45.
[8] S. T. Chang, C.-H. Wang, H. Y. Du, H. C. Hsu, C. M. Kang, C. C. Chen, J. C. S. Wu, S. C. Yen, W. F. Huang, L. C. Chen, M. C. Lin, K. H. Chen, *Energy. Environ. Sci.* **2012**, *5*, 5305.
[9] R. Jiang, D. T. Tran, J. McClure, D. Chu, *Electrochem. Commun.* **2012**, *19*, 73.
[10] R. Jiang, D. T. Tran, J. P. McClure, D. Chu, *Electrochim. Acta.* **2012**, *75*, 185.
[11] Z. X. Liang, H. Y. Song, S. J. Liao, *J. Phys. Chem. C.* **2011**, *115*, 2604.
[12] J. Liu, J. Qiu, K. Sun, J. Chen, Y. Miao, *Helv. Chim. Acta.* **2009**, *92*, 462.
[13] R. Cao, R. Thapa, H. Kim, X. Xu, M. Gyu Kim, Q. Li, N. Park, M. Liu, J. Cho, *Nat. Commun.* **2013**, *4*, 2076.
[14] Q. Wang, Z. Zhou, D. Chen, J. Lin, F. Ke, G. Xu, S. Sun, *Sci. China. Chem.* **2010**, *53*, 2057.
[15] P. B. Xi, Z. X. Liang, S. J. Liao, *Int. J. Hydrogen. Energ.* **2012**, *37*, 4606.
[16] J. B. Xu, T. S. Zhao, L. Zeng, *Int. J. Hydrogen. Energ.* **2012**, *37*, 15976.
[17] H. W. Liang, X. Cao, F. Zhou, C. H. Cui, W. J. Zhang, S. H. Yu, *Adv. Mater.* **2011**, *23*, 1467.
[18] K. Lee, L. Zhang, H. Lui, R. Hui, Z. Shi, J. Zhang, *Electrochim. Acta.* **2009**, *54*, 4704.
[19] R. Silva, D. Voiry, M. Chhowalla, T. Asefa, *J. Am. Chem. Soc.* **2013**, *135*, 7823.
[20] Y. Yuan, J. Ahmed, S. Kim, *J. Power. Sources.* **2011**, *196*, 1103.
[21] B. Winther-Jensen, O. Winther-Jensen, M. Forsyth, D. R. Macfarlane, *Science.* **2008**, *321*, 671.
[22] G. Wu, K. L. More, C. M. Johnston, P. Zelenay, *Science.* **2011**, *332*, 443.
[23] Z. Guo, Y. Qiao, H. Liu, C. Ding, Y. Zhu, M. Wan, L. Jiang, *J. Mater. Chem.* **2012**, *22*, 17153.
[24] C. Bonaventura, R. Henkens, A. I. Alayash, S. Banerjee, A. L. Crumbliss, *Antioxid. Redox. Sign.* **2013**, *18*, 2298.
[25] S. Ahmad, E. Dell'Orto, J. H. Yum, F. Kessler, M. K. Nazeeruddin, M. Graetzel, *Chem. Commun.* **2012**, *48*, 9714.
[26] L. Zhang, Y. Long, Z. Chen, M. Wan, *Adv. Funct. Mater.* **2004**, *14*, 693.
[27] F. F. Bruno, S. A. Fossey, S. Nagarajan, R. Nagarajan, J. Kumar, L. A. Samuelson, *Biomacromolecules.* **2006**, *7*, 586.
[28] H. Mao, X. Lu, D. Chao, L. Cui, Y. Li, W. Zhang, *J. Phys. Chem. C.* **2008**, *112*, 20469.
[29] D. K. Taggart, Y. Yang, S. C. Kung, T. M. McIntire, R. M. Penner, *Nano. Lett.* **2010**, *11*, 125.

DOI: 10.1002/smll.201303642

[30] B. R. Wood, S. J. Langford, B. M. Cooke, J. Lim, F. K. Glenister, M. Duriska, J. K. Unthank, D. McNaughton, *J. Am. Chem. Soc.* **2004**, *126*, 9233.
[31] J. Jang, M. Chang, H. Yoon, *Adv. Mater.* **2005**, *17*, 1616.
[32] L. Feng, Y. Yan, Y. Chen, L. Wang, *Energy. Environ. Sci.* **2011**, *4*, 1892.
[33] S. Y. Wang, D. S. Yu, L. M. Dai, D. W. Chang, J. B. Baek, *ACS Nano.* **2011**, *5*, 6202.

Received: October 25, 2013
Revised: January 9, 2014
Published online: